DOI: 10.1002/ejic.201100282

Enhanced Thermoelectric Figure of Merit of Zintl Phase $YbCd_{2-x}Mn_xSb_2$ by Chemical Substitution

Kai Guo,[a,b] Qi-Gao Cao,[a,c] Xian-Juan Feng,[a,b] Mei-Bo Tang,[a] Hao-Hong Chen,[a] Xiangxin Guo,[a] Ling Chen,[d] Yuri Grin,[e] and Jing-Tai Zhao*[a]

Dedicated to Professor John D. Corbett on the occasion of his 85th birthday

Keywords: Intermetallic phases / Thermoelectric properties / Zintl phases / Solid-state reactions / Chemical substitution

Samples of Zintl phase $YbCd_{2-x}Mn_xSb_2$ ($CaAl_2Si_2$-type, space group $P\bar{3}m1$) were prepared by a solid-state reaction followed by a suitable annealing and spark plasma sintering (SPS) for densification. Investigations were carried out on chemical substitution of Cd by Mn in order to optimize the thermoelectric figure of merit ZT in the solid solution system $YbCd_{2-x}Mn_xSb_2$ (x = 0, 0.05, 0.1, 0.15, 0.2, 0.4, 0.6, 0.8, 1.0, 1.5 and 2.0). Seebeck coefficients, electrical and thermal conductivities of all the samples were measured in the temperature range 300–650 K. The presence of Mn ($x \leq 0.2$) substantially reduces the thermal conductivity and enlarges the Seebeck coefficient, meanwhile decreasing the electrical conductivity to a certain degree. As the concentration of Mn (x) becomes higher than 1.0, the semimetallic nature of $YbCd_{2-x}Mn_xSb_2$ changes to that of a semiconductor with the majority the carriers switching from holes to electrons. Of all the samples, polycrystalline $YbCd_{1.85}Mn_{0.15}Sb_2$ (p-type charge carriers) shows the highest figure of merit ZT of 1.14 at 650 K.

Introduction

Conversion of waste heat to useful electricity becomes a potential source of energy, which can help in alleviating the energy crisis.[1–3] The heat may come from the combustion of fossil fuels, sunlight, or be a byproduct of various processes (e.g. chemical reactions and nuclear decay).[4] To utilize these forms of heat, thermoelectric (TE) materials are essential in the process of saving energy and protecting the environment.[5,6] Therefore, extensive attention has been concentrated on thermoelectric compounds to optimize the dimensionless figure of merit $ZT = S^2\sigma T/\kappa$ of the TE material, which quantifies the efficiency of a TE device (S is the Seebeck coefficient, σ the electrical conductivity, κ the thermal conductivity, and T the absolute temperature).[7] According to the formula of ZT, a good TE material with a high ZT value should reveal a combination of high electrical conductivity σ, low thermal conductivity κ, and large thermopower (absolute value of the Seebeck coefficient S). Materials that meet these requirements are found for typically heavily doped, narrow-band-gap semiconductors or semimetals.[8,9] Such systems provide a balance between the large Seebeck coefficient of semiconductors and the high electrical conductivity of metals. In addition, good TE materials are supposed to have complex crystal structures for scattering phonons, resulting in a low thermal conductivity and enhanced thermoelectric efficiency.[10]

Recently, it has been shown that several Cd- and Sb-based Zintl phase compounds,[11–14] which are representatives of the $CaAl_2Si_2$ type[15] of crystal structure (Figure 1), display novel thermoelectric properties. These layered Cd- and Sb-based intermetallics, which partly meet the above requirements, show great potential for the optimization of their thermoelectric properties by chemical tuning. $YbCd_2Sb_2$ has a maximum ZT value of 0.98 at 700 K,[11] which may be attributed to the features of heavy Sb and Yb in atomic interactions and the small difference in electronegativity between Cd and Sb, leading to a low lattice thermal conductivity and considerable electrical transport properties, respectively.[16,17] A further reduction of the thermal conductivity can be expected by partial replacement of the constituting elements to raise thermoelectric efficiency. It has been shown that the thermoelectric properties of the

[a] Key Laboratory of Transparent Opto-Functional Inorganic Materials of Chinese Academy of Sciences, Shanghai Institute of Ceramics,
1295 Dingxi Road, Shanghai 200050, P. R. China
Fax: +86-21-5243122
E-mail: jtzhao@mail.sic.ac.cn
[b] Graduate School of Chinese Academy of Sciences,
19A Yuquan Road, Beijing 100039, P. R. China
[c] Northwest Institute for Nonferrous Metal Research,
96 Weiyang Road, Xi'an 710016, Shaanxi, P. R. China
[d] Key Laboratory of Optoelectronic Materials Chemistry and Physics, Fujian Institute of Research on the Structure of Matter, Chinese Academy of Sciences,
Fuzhou, Fujian 350002, P. R. China
[e] Max-Planck-Institut für Chemische Physik fester Stoffe,
Nöthnitzer Str. 40, Dresden 01187, Germany

 © 2011 Wiley-VCH Verlag GmbH & Co. KGaA, Weinheim

respective ternary Zintl compounds can be improved within the quaternary solid solutions by substituting all the three crystallographic sites in the structure, e.g. $Ca_{1-x}Yb_xZn_2Sb_2$,[10] $Yb_xEu_{1-x}Cd_2Sb_2$,[14] $YbZn_xCd_{2-x}Sb_2$,[11] $YbZn_{2-x}Mn_xSb_2$,[18] $Yb_{1-x}Ca_xCd_2Sb_2$,[19] and $YbCd_2Sb_{2-x}Ge_x$.[20] The fact that $YbMn_2Sb_2$[21] is isostructural to $YbCd_2Sb_2$ but has different properties inspired our present study of the substitution of Cd by Mn. In this work, thermoelectric properties in the solid solutions $YbCd_{2-x}Mn_xSb_2$ with x = 0, 0.05, 0.1, 0.15, 0.2, 0.4, 0.6, 0.8, 1.0, 1.5, and 2.0 were investigated. One expects that substitution by Mn may introduce chemical disorder and influence the electron and phonon scattering, thus improving or finely tuning the thermoelectric properties of $YbCd_2Sb_2$.

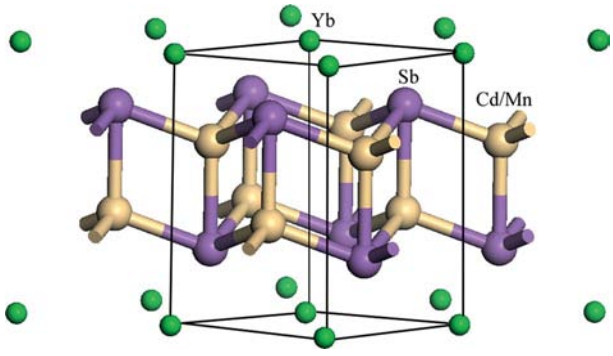

Figure 1. The crystal structure of $YbCd_{2-x}Mn_xSb_2$ ($CaAl_2Si_2$-type, $P\bar{3}m1$).

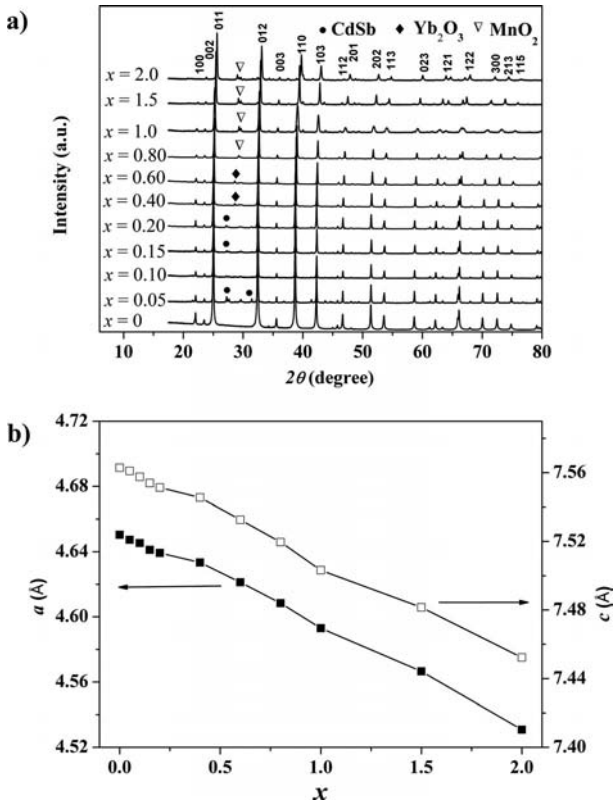

Figure 2. Powder diffraction data for $YbCd_{2-x}Mn_xSb_2$: (a) XRPD patterns for the investigated samples; (b) dependence of the unit cell parameters on the Mn content x.

Results and Discussion

The X-ray powder diffraction (XRPD) patterns of as-synthesized polycrystalline samples after spark plasma sintering (SPS) are shown in Figure 2a. The diffraction patterns of $YbCd_{2-x}Mn_xSb_2$ ($x > 0$) are similar to that of $YbCd_2Sb_2$.[22] The main diffraction peaks are indexed with a trigonal $CaAl_2Si_2$-type lattice (space group $P\bar{3}m1$), which is ubiquitous for AB_2X_2, where A is an alkaline earth or a divalent rare earth metal, B is a transition metal or a main group element, and X comes from group 15, 14, or, more rarely, 13.[23] Several additional weak reflections are also observed in the patterns when $x > 0$ (marked in Figure 2a), ascribed to traces of impurity phases such as CdSb, Yb_2O_3, and MnO_2. The experimentally obtained values of cell parameters a and c decrease monotonically with increasing Mn content (Figure 2b), indicating the effect of replacing Cd by Mn and the formation of $YbCd_{2-x}Mn_xSb_2$ solid solutions. It is expected that Mn and Cd occupy the B site concurrently, producing more chemical disorder within $YbCd_{2-x}Mn_xSb_2$. Thus, despite the unchanged valence state, the presence of Mn in lattices has an influence on the electronic structure and consequently on the thermoelectric properties, which will be discussed below.

SEM was carried out to investigate the fracture cross-sections of selected samples, as shown in Figure 3. In case of x = 0 and 0.15, although the edges of grains are obscure,

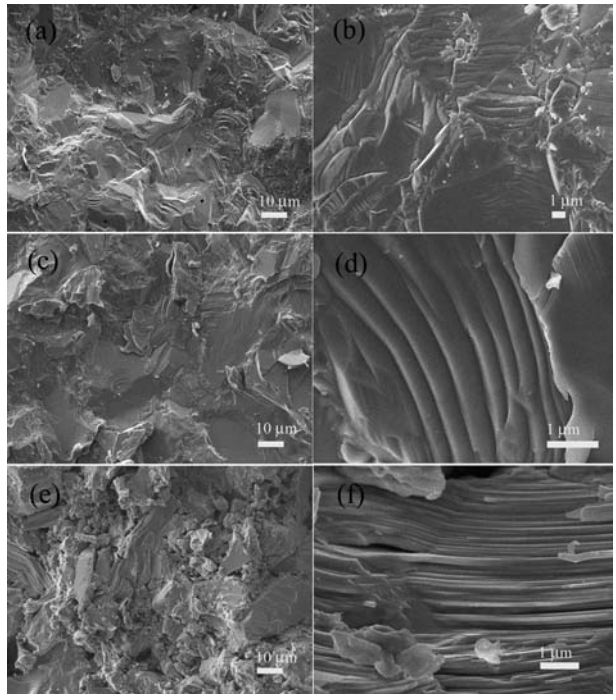

Figure 3. SEM images of the polycrystalline $YbCd_{2-x}Mn_xSb_2$ samples: (a) x = 0; (c) x = 0.15; (e) x = 2.0 in low magnification and (b) x = 0; (d) x = 0.15; (f) x = 2.0 in high magnification.

 © 2011 Wiley-VCH Verlag GmbH & Co. KGaA, Weinheim

the polycrystalline bulk seems to be compact, since only few micropores with diameters of several hundred nanometers are observed. High-magnification SEM (Figure 3b and d) reveals parallel stripes with a spacing of about 5 μm, indicating some structure of the texture in the samples. In view of the layered structure of $YbCd_{2-x}Mn_xSb_2$, it is implied that is favorable for $YbCd_{2-x}Mn_xSb_2$ to grow along the *ab* plane. A slight amount of Mn has restrained influence on the structure during the SPS process. However, the spacing between the stripes becomes narrower down to approximately 100 nm when $x = 2.0$ (Figure 3f). One can speculate that $YbMn_2Sb_2$ grows more easily into a layered structure than $YbCd_2Sb_2$, which is confirmed by repeated results. It is worth noting that the orientations of the textures are disordered in the samples (see Figure 3b), and the polycrystalline samples are considered to be isotropic as a whole to a certain degree.

The gray and dark gray regions in the back-scattered electron image for $YbCd_{1.90}Mn_{0.10}Sb_2$ indicate different phases, as can be seen in Figure 4 and Table 1. The black regions are pores in the bulk material, while the gray regions are the main phase. In addition, Sb-rich phases are detected in the dark gray regions with traces of Sb presumably located at grain boundaries.

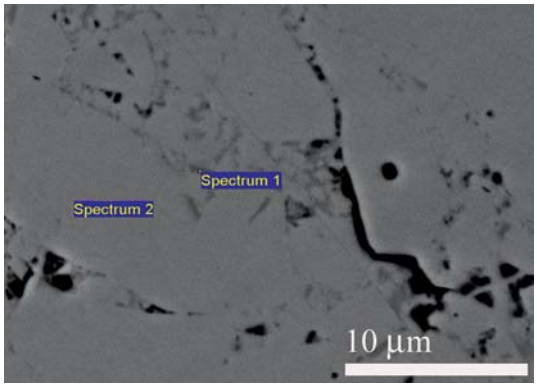

Figure 4. Back-scattered electron image of regions 1 and 2 for $YbCd_{1.90}Mn_{0.10}Sb_2$ (dark regions are open pores, dark gray inclusions represent Sb-rich phases) obtained with an energy-dispersive spectrometer.

Table 1. All elements of $YbCd_{1.90}Mn_{0.10}Sb_2$ for regions 1 and 2 shown in Figure 4 analyzed with an energy-dispersive spectrometer.

	Element	Wt.-%	Atom-%	Compositions
Spectrum 1	Mn	0.47	1.08	$Yb_{0.30}Cd_{0.32}Mn_{0.03}Sb_2$
	Cd	10.92	12.21	
	Sb	73.05	75.41	
	Yb	15.56	11.30	
Spectrum 2	Mn	0.66	1.56	$Yb_{1.30}Cd_{1.92}Mn_{0.08}Sb_2$
	Cd	31.28	36.16	
	Sb	35.35	37.72	
	Yb	32.71	24.56	

Plots of electrical conductivity (σ) of polycrystalline $YbCd_{2-x}Mn_xSb_2$ ($0 \leq x \leq 2.0$) compounds as a function of temperature over the range 300–650 K are shown in Figure 5a. The electrical conductivity decreases nearly linearly with increasing temperature if $x \leq 0.2$. In case of $0.4 \leq x \leq 1.0$, it decreases up to 550 K and then increases as the temperature increases further. For $1.5 \leq x \leq 2.0$, the electrical conductivity increases continuously with a rise in temperature for $YbCd_{2-x}Mn_xSb_2$. The observed temperature-dependent behavior of the electrical conductivity suggests a gradual change from a semimetallic $YbCd_2Sb_2$ to a typical degenerate semiconductor $YbMn_2Sb_2$. Figure 5b shows the electrical conductivity σ as a function of Mn content x at room temperature, indicating the influence of the Mn concentration on electrical transport in $YbCd_{2-x}Mn_xSb_2$. With respect to magnitude, the conductivity drops obviously as the concentration of Mn increases to $x = 0.80$, and it stays the same afterwards or increases slightly as x goes from 0.80 to 2.0. Because $YbMn_2Sb_2$ is an n-type semiconductor and thus transport properties are dominated by electron concentration (confirmed by the negative Seebeck coefficient below), quantities of Mn ($x \leq 0.60$) can lead to recombination between electrons and holes, thus reducing the hole concentration in $YbCd_2Sb_2$, which shows p-type conductivity behavior. Such results are confirmed by measure-

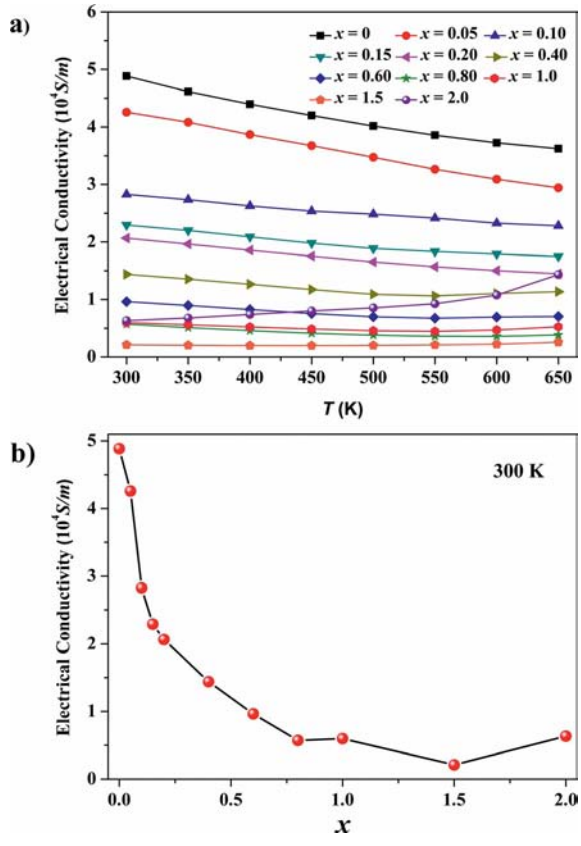

Figure 5. Electrical conductivity as a function of (a) temperature and (b) Mn concentration at room temperature.

Table 2. Carrier concentration and Hall mobility of $YbCd_{2-x}Mn_xSb_2$.

x in $YbCd_{2-x}Mn_xSb_2$	0	0.05	0.10	0.15	0.20	0.40	0.60
Carrier concentration (10^{19} cm^{-3})	4.3	3.6	2.8	2.2	2.1	1.7	1.1
Hall mobility (cm^{2}V^{-1} S^{-1})	72	73	63	64	74	54	53

 © 2011 Wiley-VCH Verlag GmbH & Co. KGaA, Weinheim

ments of the Hall mobility (Table 2). While x increases up to 2.0, the electrical conductivity is enhanced due to the more dominant carriers, the induced electrons.

The changes in the Seebeck coefficient with varying Mn content are not obvious when $x \leq 0.8$; however, the Seebeck coefficient reaches a maximum value of 259 μV/K at 650 K when $x = 0.6$ (Figure 6a). When $x = 1.50$, the values approach zero, which indicates that the effect of electrons and holes on the Seebeck coefficient are practically canceled out. For all values of x, the Seebeck coefficients exhibit a positive sign in the studied temperature range except for $x = 2.0$, which corroborates the p-type conduction for $YbCd_{2-x}Mn_xSb_2$ ($0 \leq x \leq 1.5$). In case of $YbMn_2Sb_2$ ($x = 2.0$), all Seebeck coefficients in the measured temperature range are negative, suggesting that $YbMn_2Sb_2$ is an n-type semiconductor. In the temperature range 300–500 K, the power factor $S^2\sigma$ for $YbCd_{1.95}Mn_{0.05}Sb_2$ is higher than those for other samples shown in Figure 6b. Thus, the 5% Mn substitution of Cd atoms improves the electrical transport properties, while further substitution reduces the power factor.

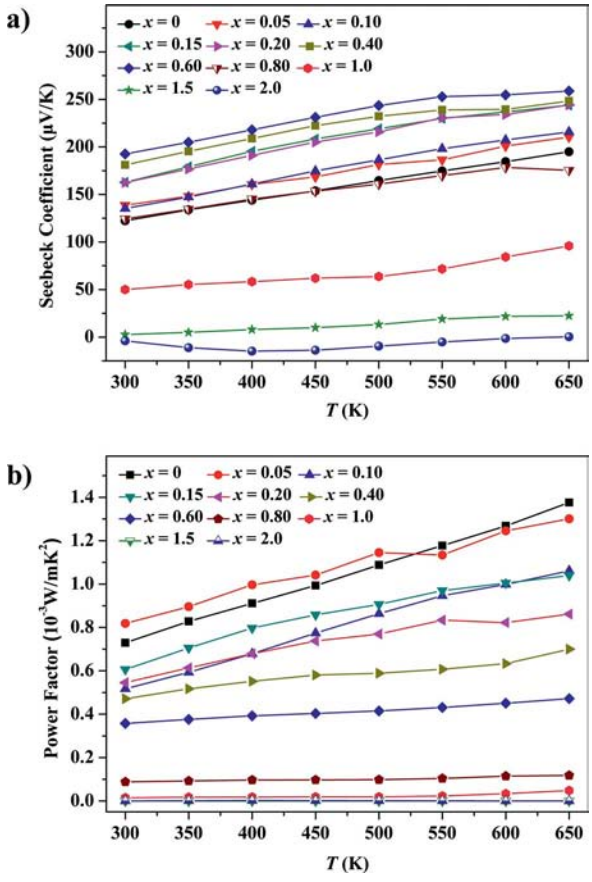

Figure 6. Temperature dependence of: (a) Seebeck coefficient S; (b) power factor $S^2\sigma$.

The total and lattice thermal conductivity of $YbCd_{2-x}Mn_xSb_2$ ($0.0 \leq x \leq 2.0$) are presented in Figure 7. $YbCd_{1.4}Mn_{0.6}Sb_2$ exhibits the lowest total thermal conductivity and $YbMn_2Sb_2$ the highest one. The partially substituted samples show much lower total thermal conductivity than pristine $YbCd_2Sb_2$ and $YbMn_2Sb_2$ (Figure 7b). This can be discussed by considering the two components of total thermal conductivity κ, lattice thermal conductivity κ_l and electronic thermal conductivity κ_e. According to the Wiedemann–Franz law, the electronic thermal conductivity is calculated by $\kappa_e = L\sigma T$ (the Lorenz number $L = \pi^2\kappa_B^2/3e = 2.4 \times 10^{-8}$ WΩK^{-2}),[24] and then the lattice thermal conductivity is evaluated as $\kappa_l = \kappa - \kappa_e$. A decrease in the electrical conductivity of $YbCd_{2-x}Mn_xSb_2$ ($0.0 \leq x \leq 1.5$) in Figure 5a results in a decrease in the electronic contribution to the total thermal conductivity. Because $YbCd_2Sb_2$ has relatively high electrical conductivity, a higher thermal conductivity is the result. Additional arguments for under-

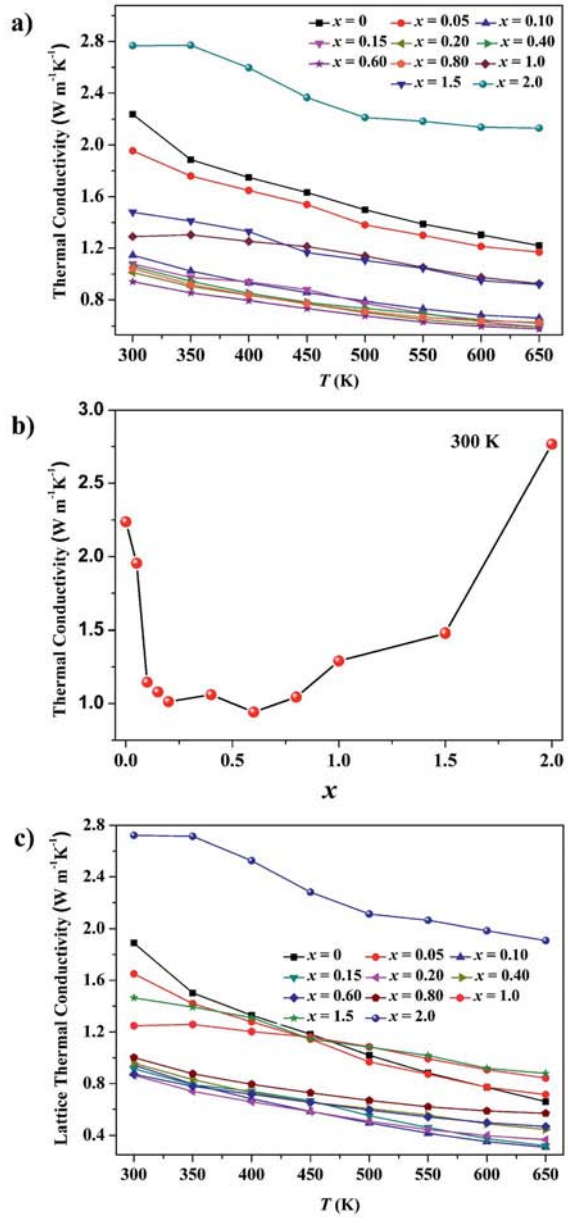

Figure 7. Total thermal conductivity for $YbCd_{2-x}Mn_xSb_2$ as a function of (a) temperature, (b) Mn content at room temperature; (c) lattice thermal conductivity for $YbCd_{2-x}Mn_xSb_2$ as a function of temperature.

 © 2011 Wiley-VCH Verlag GmbH & Co. KGaA, Weinheim

standing the variation in lattice thermal conductivity in Figure 7c are due to the disorder introduced by Mn in the crystal structure. The fluctuation of atomic size, mass, and lattice force can enhance phonon scattering and result in lower lattice thermal conductivity. Competition between these two aspects reduces the lattice thermal conductivity to a minimum value at $x = 0.1$ at high temperatures. The variation in the two components of total thermal conductivity κ, lattice thermal conductivity κ_l and electronic thermal conductivity κ_e, causes the substituted samples to show much lower thermal conductivity.

The temperature dependence of the figure of merit ZT is plotted in Figure 8. ZT increases with increasing temperature and decreases with increasing Mn content for $x \geq 0.15$, while the ZT values of $x = 0.1$, $x = 0.15$ and $x = 0.2$ are larger than that for $x = 0$. Therefore, the highest ZT value is 1.14 for $YbCd_{1.85}Mn_{0.15}Sb_2$ at 650 K, an improvement of 63% as compared with that of $YbCd_2Sb_2$. It can be further expected from the trend of the curve that the value may be higher above 650 K.

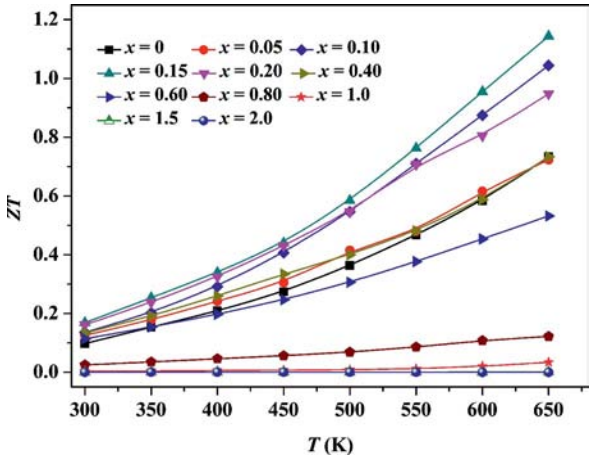

Figure 8. Temperature dependence of figure of merit ZT for $YbCd_{2-x}Mn_xSb_2$.

Conclusion

Thermoelectric materials based on Zintl phase $YbCd_{2-x}Mn_xSb_2$ ($x = 0$, 0.05, 0.1, 0.15, 0.2, 0.4, 0.6, 0.8, 1.0, 1.5, and 2.0) were synthesized by combining the direct solid-state reaction of the elements and the spark plasma sintering technology. The unit cell parameters decrease linearly with increasing concentration of Mn. The effects of substituting Cd by Mn on TE properties were investigated systematically. In all $YbCd_{2-x}Mn_xSb_2$ compounds, the maximum ZT value of 1.14 is obtained at 650 K for $YbCd_{1.85}Mn_{0.15}Sb_2$, which is greater than that for ternary compound $YbCd_2Sb_2$ at the same temperature by 63%.

Experimental Section

Samples of Zintl phase $YbCd_{2-x}Mn_xSb_2$ ($x = 0$, 0.05, 0.1, 0.15, 0.2, 0.4, 0.6, 0.8, 1.0, 1.5, and 2.0) were prepared by combined use of the direct solid-state reaction and subsequent spark plasma sintering for densification. All materials were handled in a nitrogen-filled glove box with H_2O/O_2 levels below 3.0 ppm. The mixtures of Yb (99.9%), Cd (99.999%), Mn (99.9%), and Sb (99.999%) in a molar ratio 1:(2–x):x:2 were placed in a graphite crucible with 10 mm diameter and 30 mm height, and then they were sealed into evacuated quartz tubes. These assemblies were heated slowly up to 1273 K at a rate of 1 K/min, kept for 72 h, and subsequently cooled to room temperature at a rate of 2 K/min. The products were finely powdered, pressed into pellets and annealed at 873 K for seven days. The as-obtained samples were ground in an agate mortar to fine powders. In order to obtain bulk samples, spark plasma sintering (Dr. Sinter SPS 2040 setup manufactured by Sythex SPS, Tokyo) was carried out at 753–823 K for 5 min under a uniaxial pressure of 60 MPa in vacuo. The samples showed metallic luster and stability in air. The densities of the sintered pellets were measured by the Archimedes method. The relative densities were above 93% of the theoretical values. For thermoelectric property measurements, prism-shaped specimens of average size 10 mm × ca. 2.5 mm × ca. 1.5 mm were cut from the sintered samples.

The sintered samples were characterized by X-ray powder diffraction (XRPD) with a Huber Guinier G670 Image Plate Camera (Cu-$K_{\alpha 1}$ radiation, $\lambda = 1.5406$ Å). The chemical composition of the phases was determined by using electron probe microanalysis (EPMA, 8705QH2). The microstructures of the polycrystalline $YbCd_{2-x}Mn_xSb_2$ samples were examined by scanning electron microscopy (SEM). The thermal diffusivity of specimens was determined by using a NETZSCH LFA 427 Micro Flash instrument. The thermal conductivity of the pellets can be derived from the relationship $\kappa = dC_p\lambda$, where d is the experimental density, λ is the experimental thermal diffusivity, and C_p is the heat capacity. The electrical conductivity and Seebeck coefficient were measured simultaneously under a helium atmosphere from 300 K to 650 K with an ULVAC-RIKO ZEM-3 instrument. The errors for electrical conductivity and Seebeck coefficient are estimated to be 10% and 7%, respectively. According to the thermal analysis (TG/DTA) data, $YbCd_{1.9}Mn_{0.1}Sb_2$ starts to lose weight above 700 K, which sets the temperature limit for measurements to 650 K.

Acknowledgments

We would like to thank Professor L. D. Chen of the Shanghai Institute of Ceramics of the Chinese Academy of Sciences for the thermal diffusivity measurements above room temperature. Financial support from the National Basic Research Program of China (Project No. 2007CB607503), National Natural Science Foundation of China (NSFC) (No. 50821004), the "Hundred Talent Program" of the Chinese Academy of Sciences, and the Max Planck Society–Chinese Academy of Sciences Partner Group are acknowledged.

[1] B. C. Sales, D. Mandrus, R. K. Williams, *Science* **1996**, *272*, 1325–1328.
[2] F. J. DiSalvo, *Science* **1999**, *285*, 703–706.
[3] L. E. Bell, *Science* **2008**, *321*, 1457–1461.
[4] F. J. Weinberg, D. M. Rowe, G. Min, *J. Phys. D: Appl. Phys.* **2002**, *35*, L61–L63.
[5] S. M. Kauzlarich, S. R. Brown, G. J. Snyder, *Dalton Trans.* **2007**, *21*, 2099–2107.
[6] J. R. Sootsman, D. Y. Chung, M. G. Kanatzidis, *Angew. Chem.* **2009**, *121*, 8768; *Angew. Chem. Int. Ed.* **2009**, *48*, 8616–8639.
[7] D. M. Rowe, *CRC Handbook of Thermoelectrics*, CRC, New York, **1995**.

 © 2011 Wiley-VCH Verlag GmbH & Co. KGaA, Weinheim

[8] H. Zhang, J. T. Zhao, Y. Grin, X. J. Wang, M. B. Tang, Z. Y. Man, H. H. Chen, X. X. Yang, *J. Chem. Phys.* **2008**, *129*, 164713.
[9] S. R. Brown, E. S. Toberer, T. Ikeda, C. A. Cox, F. Gascoin, S. M. Kauzlarich, G. J. Snyder, *Chem. Mater.* **2008**, *20*, 3412–3419.
[10] F. Gascoin, S. Ottensmann, D. Stark, S. M. Haile, G. J. Snyder, *Adv. Funct. Mater.* **2005**, *15*, 1860–1864.
[11] X. J. Wang, M. B. Tang, H. H. Chen, X. X. Yang, J. T. Zhao, U. Burkhardt, Y. Grin, *Appl. Phys. Lett.* **2009**, *94*, 092106.
[12] H. Zhang, L. Fang, M. B. Tang, H. H. Chen, X. X. Yang, X. Guo, J. T. Zhao, Y. Grin, *Intermetallics* **2010**, *18*, 193–198.
[13] H. Zhang, M. Baitinger, M. B. Tang, Z. Y. Man, H. H. Chen, X. X. Yang, Y. Liu, L. Chen, Y. Grin, J. T. Zhao, *Dalton Trans.* **2010**, *39*, 1101–1104.
[14] H. Zhang, L. Fang, M. B. Tang, Z. Y. Man, H. H. Chen, X. X. Yang, M. Baitinger, Y. Grin, J. T. Zhao, *J. Chem. Phys.* **2010**, *133*, 194701.
[15] E. I. Gladyshevskii, P. I. Kripyakevich, O. I. Bodak, *Ukr. Fiz. Zh. (Russ. Ed.)*. **1967**, *12*, 445.
[16] G. K. H. Madsen, *J. Am. Chem. Soc.* **2006**, *128*, 12140–12146.
[17] E. S. Toberer, A. F. May, C. J. Scanlon, G. J. Snyder, *J. Appl. Phys.* **2009**, *105*, 063701.
[18] C. Yu, T. J. Zhu, S. N. Zhang, X. B. Zhao, J. He, Z. Su, T. M. Tritt, *J. Appl. Phys.* **2008**, *104*, 013705.
[19] Q. G. Cao, H. Zhang, M. B. Tang, H. H. Chen, X. X. Yang, Y. Grin, J. T. Zhao, *J. Appl. Phys.* **2010**, *107*, 053714.
[20] Q. G. Cao, Thesis [*Preparation and Properties of YbCd(Zn)$_2$-Sb$_2$-Based Thermoelectric Materials*], Shanghai Institute of Ceramics, Chinese Academy of Science, pp. 87–99.
[21] F. Wartenberg, C. Kranenberg, R. Pocha, D. Johrendt, A. Mewis, R. D. Hoffmann, B. D. Mosel, R. Pöttgen, *Z. Naturforsch. Teil B* **2002**, *57*, 1270–1276.
[22] A. Artmann, A. Mewis, M. Roepke, G. Michels, *Z. Anorg. Allg. Chem.* **1996**, *622*, 679–682.
[23] C. Zheng, R. Hoffmann, R. Nesper, H. G. Von Schnering, *J. Am. Chem. Soc.* **1986**, *108*, 1876–1884.
[24] G. J. Snyder, E. S. Toberer, *Nat. Mater.* **2008**, *7*, 105–114.

Received: March 21, 2011
Published Online: August 2, 2011

 © 2011 Wiley-VCH Verlag GmbH & Co. KGaA, Weinheim